Solution Conformation of a Peptide Fragment Representing a Proposed RNA-Binding Site of a Viral Coat Protein Studied by Two-Dimensional NMR

Marinette van der Graaf,[‡] Carlo P. M. van Mierlo,[§,∥] and Marcus A. Hemminga*[,‡]

Departments of Molecular Physics and Biochemistry, Agricultural University, Dreijenlaan 3, 6703 HA Wageningen, The Netherlands

Received October 19, 1990; Revised Manuscript Received January 30, 1991

ABSTRACT: The first 25 amino acids of the coat protein of cowpea chlorotic mottle virus are essential for binding the encapsidated RNA. Although an α-helical conformation has been predicted for this highly positively charged N-terminal region [Argos, P. (1981) *Virology 110*, 55–62; Vriend, G., Verduin, B. J. M., & Hemminga, M. A. (1986) *J. Mol. Biol. 191*, 453–460], no experimental evidence for this conformation has been presented so far. In this study, two-dimensional proton NMR experiments were performed on a chemically synthesized pentacosapeptide containing the first 25 amino acids of this coat protein [Ten Kortenaar, P. B. W., Krüse, J., Hemminga, M. A., & Tesser, G. I. (1986) *Int. J. Pept. Protein Res. 27*, 401–413]. All resonances could be assigned by a combined use of two-dimensional correlated spectroscopy and nuclear Overhauser enhancement spectroscopy carried out at four different temperatures. Various NMR parameters indicate the presence of a conformational ensemble consisting of helical structures rapidly converting into more extended states. Differences in chemical shifts and nuclear Overhauser effects indicate that lowering the temperature induces a shift of the dynamic equilibrium toward more helical structures. At 10 °C, a perceptible fraction of the conformational ensemble consists of structures with an α-helical conformation between residues 9 and 17, likely starting with a turnlike structure around Thr9 and Arg10. Both the conformation and the position of this helical region agree well with the secondary structure predictions mentioned above.

Cowpea chlorotic mottle virus (CCMV)[1] is an icosahedral plant virus of the group of bromoviruses. It consists of RNA surrounded by 180 identical protein subunits, each 189 residues long (Dasgupta & Kaesberg, 1982). CCMV virions undergo structural changes as a function of pH, ionic strength, and temperature (Kaper, 1975). The virus particle is stable around pH 5.0, but it can be dissociated into protein dimers and RNA by raising the pH to 7.5 at high ionic strength ($I > 0.3$) (Bancroft & Hiebert, 1967). Both RNA and protein can be isolated and reassembled in vitro (Bancroft & Hiebert, 1967). In the absence of RNA, the protein subunits reassociate into empty protein capsids by lowering the pH to 5.0 (Bancroft et al., 1968). These empty protein capsids have structures similar to the native virions with a $T = 3$ icosahedral symmetry (Finch & Bancroft, 1968). The phenomena described above suggest that CCMV virus particles are stabilized by protein–RNA interactions and pH-dependent protein–protein interactions.

NMR studies on empty capsids have revealed an increased mobility of the highly basic N-terminal part of the protein subunit (Vriend et al., 1981). This mobility is absent upon binding of RNA—as in intact virions—as well as after removal of the first 25 N-terminal amino acids by tryptic digestion. Proteins lacking the N-terminal pentacosapeptide do not bind RNA (Vriend et al., 1981). This indicates that the first 25 amino acid residues (Figure 1) play an essential role in the interaction with RNA. It has been suggested that interactions between the positively charged amino acids in this part of the protein (six Arg and three Lys) and the negatively charged phosphate groups in the RNA are responsible for the protein–RNA binding (Argos, 1981; Vriend et al., 1981, 1986). This suggestion is supported by studies on brome mosaic virus (BMV), a virus closely related to CCMV. For both CCMV and BMV, the positively charged amino acids are situated in the region 7–25 within the significantly conserved first 25 amino acid residues. Sgro et al. (1986) introduced RNA–protein cross-links into brome mosaic virus by a photoreactive cross-linker with a relatively short 0.7-nm span. It was found that within the N-terminal region only residues 11–19 are involved in cross-linking with RNA. Sacher and Ahlquist (1989) investigated the effect of deletions in the N-terminal region of BMV coat protein on RNA packaging and systemic infection. From their experiments, it can be concluded that the RNA-binding region is situated somewhere in the region 8–25, which contains all but one of the positively charged amino acids.

It has been predicted that an α-helical conformation exists for the region 8–18 of BMV coat protein (Argos, 1981) and that neutralization of the positively charged arginyl and lysyl side chains initiates α-helix formation in the region 10–20 of CCMV coat protein (Vriend et al., 1986). So far, no experimental evidence for these secondary structure predictions has been presented. Laser Raman studies on CCMV have shown differences in protein structure in the presence and the absence of RNA, but no conclusions have been drawn about the nature

* Author to whom correspondence should be addressed.
‡ Department of Molecular Physics.
§ Department of Biochemistry.
∥ Present address: MRC Laboratory of Molecular Biology, Cambridge, United Kingdom.

[1] Abbreviations: 2D, two dimensional; BMV, brome mosaic virus; CCMV, cowpea chlorotic mottle virus; COSY, 2D scalar correlated spectroscopy; δ_{conf}, conformation-dependent chemical shift; $d_{\alpha\lambda}$, distance between the κ-proton of residue i and the λ-proton of residue $i + 1$; DQ, double quantum; FID, free induction decay; HoHaHa, 2D homonuclear Hartmann–Hahn transfer experiment; NMR, nuclear magnetic resonance; NOE, nuclear Overhauser enhancement; NOESY, 2D nuclear Overhauser enhancement spectroscopy; P25, synthesized N-terminal pentacosapeptide of the coat protein of CCMV; P25*, P25 containing D-valine instead of L-valine at position 3; ppm, parts per million; RNA, ribonucleic acid.

0006-2960/91/0430-5722$02.50/0

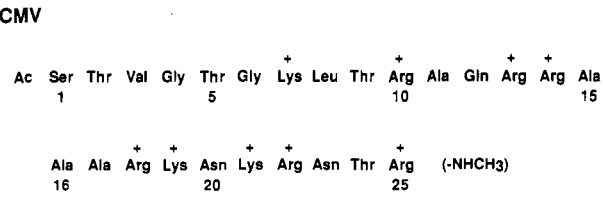

FIGURE 1: Amino acid sequence of the N-terminal arm of CCMV coat protein (Dasgupta & Kaesberg, 1982). Positively charged residues are labeled with (+) symbols. The methylamide group is present at the C-terminus of the chemically synthesized peptide P25.

of the secondary structure of the N-terminus (Verduin et al., 1984). High-resolution X-ray crystallographic structures have been obtained for a number of spherical RNA viruses: tomato bushy stunt virus (Harrison et al., 1978), southern bean mosaic virus (Abad-Zapatero et al., 1980), satellite tobacco necrosis virus (Liljas et al., 1982), human common cold virus (Rossmann et al., 1985), turnip crinkle virus (Hogle et al., 1986), and black beetle virus (Hosur et al., 1987). In all structures, the N-terminal basic arms could not, or only partly, be observed due to a lack of crystallographic symmetry. Therefore, it seems unlikely that the secondary structure of the N-terminal arm of CCMV can be obtained by X-ray diffraction techniques. High-resolution NMR experiments have provided some information about the behavior of the N-terminal arm of CCMV coat protein (Vriend et al., 1981, 1986). However, the lines in the NMR spectra are strongly broadened due to the size of the intact virus particles or protein–nucleotide complexes, which makes it extremely difficult to investigate the secondary structure of the N-terminus in these systems by NMR.

Chemical synthesis of the N-terminal pentacosapeptide P25 (Ten Kortenaar et al., 1986) has created the possibility to perform detailed NMR and optical spectroscopic studies on the structure of this N-terminal segment in the absence and the presence of nucleotides. It has been shown that the ^{1}H NMR spectrum of P25 closely resembles the ^{1}H NMR difference spectrum of intact coat protein and coat protein lacking the N-terminal region (Hemminga et al., 1985). Therefore, we have used P25 as a model for the N-terminal part of CCMV coat protein.

The objective of the study reported here is the determination of the secondary structure of the synthetic N-terminus P25 in aqueous solution by 2D proton NMR. The experiments indicate the presence of a conformational ensemble consisting of helical structures rapidly converting into more extended conformational states. It will be shown that the helical region is situated between residues 9 and 17, which agrees well with the secondary structure predictions by Argos (1981) and Vriend et al. (1986).

Materials and Methods

The N-terminal pentacosapeptide of the coat protein of CCMV was available as the chemically synthesized $N^{\alpha 1}$-acetyl-$C^{\alpha 25}$-methylamide P25 (Ten Kortenaar et al., 1986). Samples for 2D NMR measurements contained 6–8.5 mM P25 and 200 mM sodium phosphate in a mixture of 10%(v/v) ^2H_2O and 90%(v/v) H_2O, pH 4.0. This low pH value was chosen to be close to the pH minimum for the rate of chemical exchange of labile protons from amide and guanidinium groups of the peptide with the bulk water (Wüthrich & Wagner, 1979). Sodium 3-(trimethylsilyl)[2,2,3,3-$^2H_4$]propionate was used as an internal standard.

All 2D NMR spectra were recorded on a Bruker AM600 spectrometer operating at 600 MHz for protons, interfaced with an Aspect 3000 computer. The carrier frequency was chosen in the middle of the spectrum coinciding with the water resonance. The water signal was suppressed by gated irradiation or in the case of some of the NOESY spectra by using a $(90°)_\phi$–τ–$(90°)_{-\phi}$–jump–return read pulse (Plateau & Guéron, 1982) with τ = 80 μs. All spectra were acquired in the phase-sensitive mode using time proportional phase increments (Marion & Wüthrich, 1983). Spectral widths were generally about 20 ppm in the ω_2 dimension and 10 ppm in the ω_1 dimension. The spectral width in the ω_2 dimension was doubled to obtain a more flattened base line at the position of the resonance peaks. After the first Fourier transformation, the range of the spectrum containing the resonance peaks was selected and further processed. Spectra were generally recorded with 2048 or 4096 data points and 512 t_1 increments. The number of scans per t_1 increment varied between 24 and 48.

The double quantum filtered COSY spectrum (Rance et al., 1983) shown in this paper was recorded with a spectral width of approximately 10 ppm in the ω_2 dimension and 8192 data points to obtain the best possible digital resolution. The number of t_1 increments was 700. The relaxation delay period was randomly varied between 2.88 and 3.12 s to avoid the appearance of double quantum cross-peaks. The spectrum was recorded at 10 °C, since at this temperature the cross-peaks in the fingerprint region (ω_1 = 3.9–4.9 ppm, ω_2 = 7.9–8.9 ppm) show minimal overlap.

2D homonuclear Hartmann–Hahn (HoHaHa) spectra were recorded at 2, 5, 10, and 25 °C with an 80-ms MLEV17 mixing scheme (Bax & Davis, 1985). The MLEV17 cycle was preceded and followed by 2.5-ms trim pulses to defocus magnetization not parallel to the spin-lock axis. The relaxation delay was 2.5 s.

NOESY spectra (Jeener et al., 1979; Macura & Ernst, 1980) were recorded at 2, 5, 10, and 25 °C with a mixing time of 200 ms. At 10 °C, also mixing times of 50, 100, and 150 ms were used. No zero quantum suppression technique was applied. The relaxation delay was 2.5 s.

2D NMR data were processed on a MicroVAX II or a VAXstation 2000 using software kindly given by Dr. R. Boelens. The free induction decays were multiplied by shifted sine-bell window functions in both dimensions. After zero filling and double Fourier transformation, base-line corrections with a fourth-order polynomial (Pearson, 1977) were performed in both dimensions. Digital resolution in the final transformed spectrum was usually 3.13 or 6.26 Hz/point in the ω_2 dimension and 6.26 Hz/point in the ω_1 dimension. The digital resolution of the DQ-filtered COSY spectrum was 0.78 Hz/point in the ω_2 dimension and 1.57 Hz/point in the ω_1 dimension.

Results

Resonance Assignment. The assignments of the ^{1}H NMR resonances of P25 presented in Table I were obtained by using the sequential assignment methodology developed by Wüthrich and co-workers (Billeter et al., 1982; Wagner & Wüthrich, 1982; Wider et al., 1982; Wüthrich et al., 1982; Wüthrich, 1986). During the first stage of this procedure, complete spin systems of individual amino acid residues were identified by using DQ-filtered COSY and HoHaHa spectra. The next step was the establishment of connectivities across the peptide bond, which can be observed in NOESY spectra. Figure 2 shows the sequential d_{NN}, $d_{\alpha N}$, $d_{\beta N}$, and $d_{\gamma N}$ connectivities appearing in NOESY spectra recorded at 10 and 2 °C. The use of spectra recorded at different temperatures was essential in the assignment procedure, because degeneracies of resonances at one temperature often disappeared at another temperature.

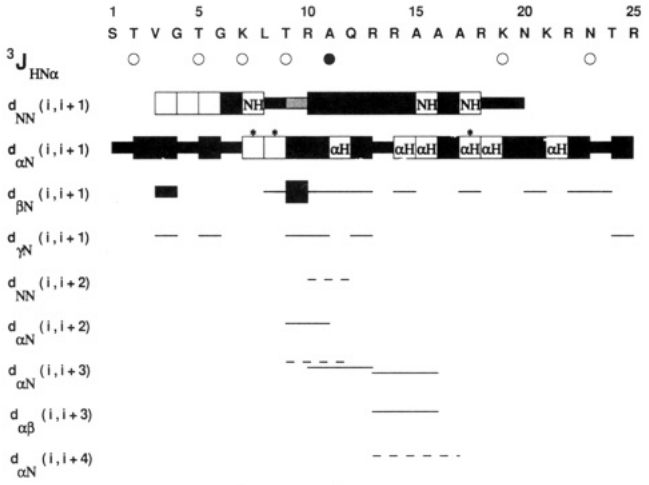

FIGURE 2: Summary of $^3J_{HN\alpha}$ coupling constants observed for P25 at 10 °C, and short- and medium-range NOEs observed at 10 and 2 °C. Open and closed circles indicate $^3J_{HN\alpha}$ coupling constants larger than 7 Hz and smaller than 6 Hz, respectively. The thickness of the lines is proportional to the NOE intensity. Open squares indicate that the presence of the connectivity is ambiguous due to overlap problems. In the case of degeneracy of the sequential NH or αH resonances, the open square contains "NH" or "αH", respectively. An asterisk above an open square indicates that the connectivity is clearly present at lower temperature than 10 °C. The dashed lines and the grey box indicate NOEs absent at 10 °C but present at 2 °C. The presented NOEs were derived from NOESY spectra recorded with mixing times of 200 ms. All presented connectivities were also observed in NOESY spectra recorded with smaller mixing times.

Figure 3A shows the assignments in the fingerprint region of a DQ-filtered COSY spectrum recorded at 10 °C, and Figure 3B shows the sequential assignment pathway form Ser1 to Arg10 in the corresponding region of a NOESY spectrum. In Figure 3A, the resonances labeled with asterisks correspond to a second set of the first six amino acids in the N-terminal region of P25. Analysis of the sample by an enantioseparation (Fujiwara et al., 1987; Brückner et al., 1989) revealed that 25–30% of the valine residues had been converted from L-valine to D-valine during the synthesis of P25. Therefore, the additional resonances were assigned to P25*, which can be defined as P25 containing D-valine instead of L-valine at position 3. Since the resonances of P25 could be separated from those of P25*, no attention will be paid to the presence of P25* in the further analysis.

Presence of Secondary Structure. The short- and medium-range NOESY connectivities presented in Figure 2 are somewhat ambiguous with respect to the secondary structure of P25. The rather intense sequential $d_{\alpha N}$ connectivities are characteristic of extended structure, and the sequential d_{NN} connectivities are characteristic of folded structures (Wüthrich, 1986). All the medium-range NOESY connectivities in the region between residues 9 and 17 are typical of a helical conformation (Wüthrich, 1986). The connectivity $d_{\alpha\beta}(8,12)$ and NOEs from side-chain resonances of Leu8 and Thr9 to side-chain resonances of Gln12 are also indicative for the presence of helical secondary structure in the region in the middle of P25.

The chemical shifts presented in Table I provide additional evidence for the presence of secondary structure in the region in the middle of P25 (residues 8–17). Several chemical shifts clearly deviate from their random-coil values, and some normally degenerate resonances are separated. For instance, the δ-protons of Leu8 have distinct resonance positions indicating that each proton experiences its own evironment. The same applies to the δ-protons of Arg13. The chemical shifts of the backbone protons differ in varying degrees from their random-coil values. Figure 4 shows the conformation-dependent chemical shifts of the α-protons at 2 and 25 °C, which were obtained by subtraction of the corresponding "random-coil" chemical shifts (Bundi & Wüthrich, 1979) from the observed shifts. Positive and negative values indicate shifts to lower and higher field, respectively. The conformation-dependent chemical shifts measured at 5 and 10 °C have values between the upper and lower limits of the shifts presented in Figure 4.

Table I: ^{1}H Chemical Shifts (ppm) of P25 in 200 mM Sodium Phosphate Buffer, pH 4.0, 10 °C

residue	NH	αH	βH	others
(Ac)				Ac-CH_3 2.08
Ser1	8.45	4.50	3.91, 3.86	
Thr2	8.41	4.45	4.30	γCH_3 1.21
Val3	8.21	4.14	2.10	γCH_3 0.97, 0.97
Gly4	8.63	4.05		
Thr5	8.22	4.36	4.31	γCH_3 1.23
Gly6	8.59	3.98		
Lys7	8.23	4.32	1.83, 1.75	γCH_2 1.44, 1.39
				δCH_2 1.68, 1.68
				εCH_2 3.01, 3.01
				ζNH_3^+ 7.61[a]
Leu8	8.29	4.56	1.67, 1.57	γCH 1.68
				δCH_3 0.89, 0.84
Thr9	8.57	4.39	4.56	γCH_3 1.30
Arg10	8.84	4.05	1.89, 1.89	γCH_2 1.77, 1.63
				δCH_2 3.24, 3.24
				εNH 7.38
Ala11	8.52	4.16	1.43	
Gln12	8.10	4.16	2.27, 2.04	γCH_2 2.44, 2.44
				δNH_2 7.60, 6.89
Arg13	8.59	4.12	1.90, 1.90	γCH_2 1.77, 1.63
				δCH_2 3.25, 3.19
				εNH 7.23
Arg14	8.33	4.18	1.89, 1.89	γCH_2 1.78, 1.64
				δCH_2 3.22, 3.22
				εNH 7.35
Ala15	8.08	4.19	1.47	
Ala16	8.06	4.20	1.45	
Ala17	7.96	4.26	1.47	
Arg18	7.99	4.25	1.91, 1.85	γCH_2 1.76, 1.67
				δCH_2 3.23, 3.23
				εNH 7.32
Lys19	8.12	4.25	1.87, 1.82	γCH_2 1.51, 1.43
				δCH_2 1.71, 1.71
				εCH_2 3.01, 3.01
				ζNH_3^+ 7.61[a]
Asn20	8.34	4.69	2.87, 2.80	γNH_2 7.70, 7.01
Lys21	8.29	4.30	1.88, 1.80	γCH_2 1.47, 1.44
				δCH_2 1.70, 1.70
				εCH_2 3.02, 3.02
				ζNH_3^+ 7.61[a]
Arg22	8.41	4.31	1.88, 1.81	γCH_2 1.68, 1.63
				δCH_2 3.22, 3.22
				εNH 7.28
Asn23	8.58	4.80	2.82, 2.90	γNH_2 7.72, 6.99
Thr24	8.25	4.34	4.27	γCH_3 1.21
Arg25	8.39	4.28	1.87, 1.79	γCH_2 1.67, 1.61
				δCH_2 3.22, 3.22
				εNH 7.27
($NHCH_3$)	7.97			CH_3 2.75

[a] The Lys ζNH_3^+ resonance is broadened around 7.61 ppm due to exchange.

Discussion

Nature of the Conformation of P25 in Aqueous Solution. The results show a simultaneous presence of $d_{\alpha N}$ and d_{NN} NOEs with almost the same intensities. It is often found that sequential NOEs characteristic of both α and β conformations are present for a small flexible peptide. An explanation for this phenomenon is conformational averaging on the NMR time scale (Wright et al., 1988). The measured NMR pa-

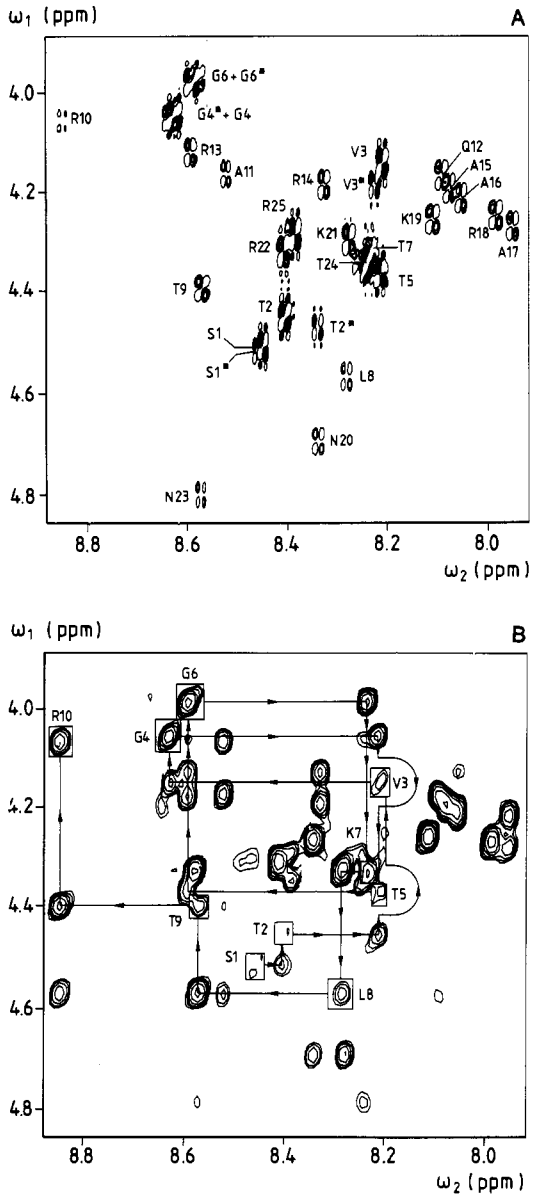

FIGURE 3: (A) Fingerprint region (ω_1 = 3.9–4.9 ppm, ω_2 = 7.9–8.9 ppm) of a 600-MHz DQ-filtered COSY spectrum of P25 recorded at 10 °C. The time domain data were multiplied by a sine-bell window function shifted by $\pi/12$ in the t_2 direction and by a sine-bell window function shifted by $\pi/6$ in t_1 direction. The digital resolution in the transformed spectrum is 0.78 Hz/point in the ω_2 dimension and 1.57 Hz/point in the ω_1 dimension. Positive peaks are represented as filled circles and negative peaks as open circles. The NH–αH cross-peaks are identified by labels. Labels with asterisks refer to P25* (see text). The NH–αH cross-peak of T5* of P25* is not labeled for reason of clarity; this cross-peak overlaps with the NH–αH cross-peaks of T24 and T7 of P25. (B) Part of a 600-MHz NOESY spectrum of P25 recorded at 10 °C with a mixing time of 200 ms. The time domain data consisting of 512 FIDs of 2K data points were multiplied by a sine-bell window function shifted by $\pi/6$ in both dimensions. The digital resolution in the transformed spectrum is 6.26 Hz/point for both dimensions. The sequential assignment pathway from S1 to R10 is indicated by arrows leading from the intraresidual $(NH–\alpha H)_i$ cross-peak via the sequential $d_{\alpha N}$ connectivity to the intraresidual $(NH–\alpha H)_{i+1}$ cross-peak. The intraresidual NH–αH cross-peaks indicated by rectangles are labeled. The spectral region overlaps with the fingerprint region (ω_1 = 3.9–4.9 ppm, ω_2 = 7.9–8.9 ppm) of the DQ-filtered COSY spectrum shown in (A).

rameters such as NOE intensities, coupling constants, and chemical shifts are a population-weighted average over all conformations sampled. Since P25 is a small and flexible peptide in aqueous solution, it is suggested that P25 samples different conformations on the NMR time scale. The strong

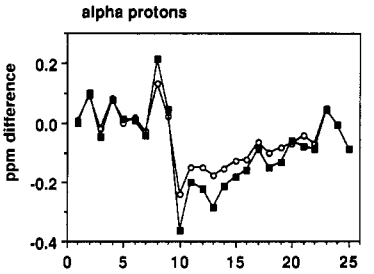

FIGURE 4: Conformation-dependent chemical shifts of α-protons at 2 °C (■) and 25 °C (○) presented as function of residue numbers. These conformation-dependent chemical shifts were obtained by subtraction of the corresponding "random-coil" chemical shifts (Bundi & Wüthrich, 1979) from the measured chemical shifts. The chemical shift values of the α-protons of T24 and R25 could not be determined at 25 °C because of overlap problems.

intensities of several αN connectivities indicate the presence of extended structures. Several medium-range NOEs characteristic of helical conformation show that a perceptible fraction of the conformational ensemble of P25 consists of structures with a helical conformation in the region in the middle of P25 (see next paragraph).

Figure 4 shows that the values of δ_{conf} of the α-protons are larger at 2 °C than at 25 °C. Furthermore, at 2 °C, the NOE connectivities $d_{NN}(9,10)$, $d_{NN}(10,12)$, $d_{\alpha N}(9,12)$, and $d_{\alpha N}(13,17)$ appear in addition to the connectivities present at 10 °C (see Figure 2). These observations indicate a shift of the dynamic conformational equilibrium toward more helical conformations by a decrease of temperature. The same phenomenon has been reported for the C-peptide (residues 1–13) and S-peptide (residues 1–20) of RNase A, which show significant α-helix formation in aqueous solution near 0 °C (Brown & Klee, 1971; Bierzynski et al., 1982; Kim & Baldwin, 1984).

Position of the Helical Region. For the region Thr9–Ala17, several medium-range NOESY connectivities characteristic of α-helical conformation such as $d_{\alpha N}(i,i+3)$, $d_{\alpha\beta}(i,i+3)$, and $d_{\alpha N}(i,i+4)$ (Wüthrich, 1986) are observed: $d_{\alpha N}(10,13)$, $d_{\alpha N}(13,16)$, and $d_{\alpha\beta}(13,16)$ at 10 °C, and also $d_{\alpha N}(9,12)$ and $d_{\alpha N}(13,17)$ at 2 °C. The connectivity $d_{\alpha N}(9,11)$ is not typical of an α-helix but indicates a 3_{10}-helix or a reverse turn (Wüthrich et al., 1984). We also note that $d_{\beta N}(9,10)$ is much stronger than the other $d_{\beta N}(i,i+1)$ connectivities. These $d_{\beta N}(i,i+1)$ connectivities are commonly observed in helical structures and tight turns (Wüthrich et al., 1984). The presence of $d_{\alpha N}(9,11)$ and the fact that $d_{\beta N}(9,10)$ is much stronger than the $d_{\beta N}(i,i+1)$ connectivities in the rest of the helical region suggest a turnlike conformation around Thr9 and Arg10.

Most $^3J_{HN\alpha}$ spin–spin coupling constants have values between 6 and 7 Hz (see Figure 2). These values could indicate a random-coil conformation, but for the region in the middle of P25, a conformational averaging between a helical ($^3J_{HN\alpha} \leq 5$) and an extended β conformation ($^3J_{HN\alpha} \geq 8$) is a more reasonable explanation. If P25 had entirely a random-coil conformation, no medium-range NOESY connectivities characteristic of a helical conformation would be present at all.

The δ_{conf} values presented in Figure 4 provide additional information about the backbone conformation of P25. In general, chemical shift information has been considered to be not very reliable because of a high sensitivity to ring-current fields of aromatic amino acids and shielding effects resulting from secondary and tertiary structure. However, P25 contains no aromatic amino acids and is too small to obtain tertiary structure. Therefore, in our case, the chemical shifts are only

influenced by local electronic structure, protonation equilibria, hydrogen bonding, and shielding effects that result from the secondary structure (Wüthrich, 1986).

It has been shown by statistical analysis of chemical shift distributions in 32 polypeptides and proteins that the α-protons of aliphatic amino acids in α-helical conformations shift upfield by 0.4 ppm, on the average (Szilágyi & Jardetzky, 1989). Figure 4 shows the largest negative values of δ_{conf} corresponding with upfield shifts between residues 10 and 13, and gradually decreasing negative values going from Arg10 in the direction of the C-terminus. The negative values between residues 10 and 20 suggest that in this region (particularly close to residue 10) an α-helical conformation is favored, in agreement with the observed medium-range NOEs.

All the phenomena described above indicate that structures with a helical conformation between residues 9 and 17 are present in the conformational ensemble. Both termini of the peptide are assumed to have random-coil conformations.

Factors Playing a Role in Helix Formation. Presta and Rose (1988) have presented a helix hypothesis based on hydrogen bond formation at the helix termini: a necessary condition for helix formation is the presence of residues whose side chains can form hydrogen bonds with the initial four helix N–H groups and final four C=O groups. In P25, the side chains of Thr9 and Gln12 can serve as hydrogen bond acceptors at the N-terminus of the helical region, and the side chains of all amino acids between residue 18 and 25 (Arg, Lys, Asn, and Thr) can serve as hydrogen bond donors at the C-terminus of the helical region. Although only two hydrogen bond acceptors are present at the N-terminus of the helical region instead of four, the helix hypothesis seems to be applicable to P25.

The α-helical region in P25 has an amphipathic character. At the hydrophobic side of this amphipathic helix, hydrophobic interactions between side chains may play a role in stabilization of the α-helix (Lim, 1974a,b). However, at the hydrophilic side, all positive charges are in close spatial proximity of each other, which is expected to be energetically unfavorable. Circular dichroism experiments have shown that addition of salt or (oligo)phosphates induces an increase of α-helical conformation in P25 (unpublished results). Furthermore, previous secondary structure predictions suggested a random-coil conformation for the N-terminal arm of CCMV coat protein with charged side chains, but an α-helix between residues 10 and 20 after charge neutralization (Vriend et al., 1986). This indicates that shielding of the positive charges neutralizes their destabilizing effect on α-helix formation. In CCMV virus particles, the positive charges are neutralized by the negatively charged phosphate groups of the encapsidated RNA. Therefore, all samples used for the NMR experiments presented here contained 200 mM sodium phosphate.

It can be concluded that P25 alternates among helical and extended backbone conformations on the NMR time scale. Under our experimental conditions, a perceptible fraction of the conformational ensemble consists of structures with an α-helical conformation between residues 9 and 17, likely starting with a turnlike structure around Thr9 and Arg10. Both position and conformation agree well with previous secondary structure predictions (Argos, 1981; Vriend et al., 1986). The amino acid sequence in the region 9–18 in CCMV is exactly the same as in BMV, for which virus it has been shown that residues 11–19 are involved in RNA binding (Sgro et al., 1986; Sacher & Ahlquist, 1989). Therefore, we suggest that the ability to form an α-helix in this region may be an essential part of the synergistic interaction with RNA.

Acknowledgments

We thank Dr. S. S. Wijmenga and J. J. M. Joordens of the SON HF-NMR Facility Nijmegen (The Netherlands) for assistance in recording the NMR spectra and C. J. A. M. Wolfs and Dr. P. B. W. ten Kortenaar for performing chemical analyses of P25.

References

Abad-Zapatero, C., Abel-Meguid, S. S., Johnson, J. E., Leslie, A. G. W. Rayment, I., Rossmann, M. G., Suck, D., & Tsukinara, T. (1980) *Nature 286*, 33–39.

Argos, P. (1981) *Virology 110*, 55–62.

Bancroft, J. B., & Hiebert, E (1967) *Virology 32*, 354–356.

Bancroft, J. B., Wagner, G. W., & Bracker, C. E. (1968) *Virology 36*, 146–149.

Bax, A., & Davis, D. G. (1985) *J. Magn. Reson. 65*, 355–360.

Bierzynski, A., Kim, P. S., & Baldwin, R. L. (1982) *Proc. Natl. Acad. Sci. U.S.A. 79*, 2470–2474.

Billeter, M., Braun, W., & Wüthrich, K. (1982) *J. Mol. Biol. 155*, 321–346.

Brown, J. E., & Klee, W. A. (1971) *Biochemistry 10*, 470–476.

Brückner, H., Wittner, R., & Godel, H (1989) *J. Chromatogr. 476*, 73–82.

Bundi, A., & Wüthrich, K. (1979) *Biopolymers 18*, 285–297.

Dasgupta, R., & Kaesberg, P. (1982) *Nucleic Acids Res. 10*, 703–713.

Finch, J. T., & Bancroft, J. B. (1968) *Nature 220*, 815–816.

Fujiwara, M., Ishida, Y., Nimura, N., Toyama, A., & Kinoshita, T. (1987) *Anal. Biochem. 166*, 72–78.

Harrison, S. C., Olson, A. J., Schutt, C. E., Winkler, F. K., & Bricogne, G. (1978) *Nature 276*, 368–373.

Hemminga, M. A., Datema, K. P., ten Kortenaar, P. W. B., Krüse, J., Vriend, G., Verduin, B. J. M., & Koole, P. (1985) in *Magnetic Resonance in Biology and Medicine* (Govil, G., Khetrapal, C. L., Saran, A., Eds.) pp 53–76, Tata McGraw-Hill, New Delhi.

Hogle, J. M., Maeda, A., & Harrison, S. C. (1986) *J. Mol. Biol. 159*, 93–108.

Hosur, M. V., Schmidt, T., Tucker, R. C., Johnson, J. E., Gallagher, T. M., Selling, B. H., & Ruekert, R. R. (1987) *Proteins: Struct., Funct., Genet. 2*, 167–176.

Jeener, J., Meier, B. H., Bachmann, P., & Ernst, R. R. (1979) *J. Chem. Phys. 71*, 4546–4553.

Kaper, J. M. (1975) *The Chemical Basis of Virus Structure, Dissociation and Reassembly*, North-Holland, Amsterdam.

Kim, P. S., & Baldwin, R. L. (1984) *Nature 307*, 329–334.

Liljas, L., Unge, T., Jones, T. A., Fridborg, K., Lövgren, S., Skoglund, U., & Strandberg, B. (1982) *J. Mol. Biol. 159*, 93–108.

Lim, V. I. (1974a) *J. Mol. Biol. 88*, 857–872.

Lim, V. I. (1974b) *J. Mol. Biol. 88*, 873–894.

Macura, S., & Ernst, R. R. (1980) *Mol. Phys. 41*, 95–117.

Marion, D., & Wüthrich, K. (1983) *Biochem. Biophys. Res. Commun. 113*, 967–974.

Pearson, G. A. (1977) *J. Magn. Reson. 27*, 265–272.

Plateau, P., & Guéron, M. (1982) *J. Am. Chem. Soc. 104*, 7310–7311.

Presta, L. G., & Rose, G. D. (1988) *Science 240*, 1632–1641.

Rance, M., Sørensen, O. W., Bodenhausen, G., Wagner, G., Ernst, R. R., & Wüthrich, K. (1983) *Biochem. Biophys. Res. Commun. 117*, 479–485.

Rossmann, M. G., Arnold, E., Erickson, J. W., Frankenberger, E. A., Griffith, J. P., Hecht, H. J., Johnson, J. C., Kamer, G., Luo, M., Mosser, A. G., Rueckert, R. R., Sherry, B., & Vriend, G. (1985) *Nature 317*, 145–153.

Sacher, R., & Ahlquist, P. (1989) *J. Virol. 63*, 4545-4552.
Sgro, J., Jacrot, B., & Chroboczek, J. (1986) *Eur. J. Biochem. 154*, 69-76.
Szilágyi, L., & Jardetzky, O. (1989) *J. Magn. Reson. 83*, 441-449.
Ten Kortenaar, P. B. W., Krüse, J., Hemminga, M. A., & Tesser, G. I. (1986) *Int. J. Pept. Protein Res. 27*, 401-413.
Verduin, B. J. M., Prescott, B., & Thomas, G. J., Jr. (1984) *Biochemistry 23*, 4301-4308.
Vriend, G., Hemminga, M. A., Verduin, B. J. M., de Wit, J. L., & Schaafsma, T. J. (1981) *FEBS Lett. 134*, 167-171.
Vriend, G., Verduin, B. J. M., & Hemminga, M. A. (1986) *J. Mol. Biol. 191*, 453-460.
Wagner, G., & Wüthrich, K. (1982) *J. Mol. Biol. 155*, 347-366.
Wider, G., Lee, K. H., & Wüthrich, K. (1982) *J. Mol. Biol. 155*, 367-388.
Wright, P. E., Dyson, H. J., & Lerner, R. A. (1988) *Biochemistry 27*, 7167-7175.
Wüthrich, K. (1986) *NMR of Proteins and Nucleic Acids*, Wiley, New York.
Wüthrich, K., & Wagner, G. (1979) *J. Mol. Biol. 130*, 1-18.
Wüthrich, K., Wider, G., Wagner, G., & Braun, W. (1982) *J. Mol. Biol. 155*, 311-319.
Wüthrich, K., Billeter, M., & Braun, W. (1984) *J. Mol. Biol. 180*, 715-740.

Reaction of Hydrogen Peroxide with the Rapid Form of Resting Cytochrome Oxidase†

Lichun Weng and Gary M. Baker*
Department of Chemistry, Northern Illinois University, DeKalb, Illinois 60115
Received November 28, 1990; Revised Manuscript Received March 7, 1991

ABSTRACT: The hydrogen peroxide binding reaction has been examined with alkaline-purified resting enzyme in order to avoid mixtures of low pH induced fast and slow conformers. At pH 8.8–9.0 (20 °C), the reactivity of resting enzyme was similar to the peroxide-free, pulsed conformer that has been characterized by other investigators. The reaction showed single-phase reactivity at 435 and 655 nm and required a minimum 8:1 molar excess of peroxide (over cytochrome a_3) for quantitative reaction. At 16:1, the Soret band was stable for 1.0–1.5 h, but above 80:1, the band began showing generalized attenuation within 1–2 min. The peroxide binding reaction was also associated with an increase in absorbance at 606 nm which correlated with the rate of change at 435 and 655 nm. The observed rate constants at each of these wavelengths showed similar linear dependence on peroxide concentration, giving an average bimolecular rate constant of 391 $M^{-1}\cdot s^{-1}$ and a K_d of 5.1 μM. The rise phase at 606 nm was observed to saturate at an 8:1 molar excess of peroxide but showed a slow, concentration-dependent first-order decay that gave a bimolecular rate constant and K_d of 38 $M^{-1}\cdot s^{-1}$ and 20 μM, respectively. The decay was not associated with a change in the Soret absorption or charge-transfer regions, suggesting a type of spectral decoupling. An isosbestic point at 588 nm was consistent with the 606- to 580-nm conversion proposed by other investigators, although direct observation of a new band at 580 nm was difficult. The insensitivity of the Soret band to the loss of absorbance at 606 nm implies that the 606- and 580-nm species do not differ in oxidation state, contrary to the structural assignments made by other investigators. The decay at 606 nm is proposed to be associated with a chemical event at a non-heme site, possibly Cu_B or one of its ligands.

Ligand binding studies of cytochrome *c* oxidase (EC 1.9.3.1) have been complicated by enzyme heterogeneity, particularly in preparations derived from cholate and ammonium sulfate [for recent discussions, see Hartzell et al. (1988), Beinert (1988), and Malmström (1990)]. The reaction of hydrogen peroxide with resting enzyme illustrates the type of problem encountered. For example, a 10-fold molar excess of peroxide was reported by Bickar et al. (1982) to induce only a partial red shift in the Soret band from 417 to 422 nm, but substantial preparation-dependent differences were also observed. Using similar conditions, Vygodina and Konstantinov (1988) observed the band to shift much further, to 427–428 nm. Wrigglesworth (1984) observed a comparable shift, but only with much higher levels of peroxide.

The kinetics in the Soret region also reveal discrepancies. For example, peroxide binding to resting enzyme was shown by Gorren et al. (1986) to consist of a rapid phase followed by a peroxide-independent slow phase, whereas Bickar et al. (1985) have reported three separate phases, each dependent on peroxide concentration.

Variable observations are also evident in the visible region. Witt and Chan (1987) reported a peroxide-induced α-band at 596 nm, whereas other investigators, using either resting or pulsed enzyme, have found this band to be more red-shifted, at 600–601 nm (Bickar et al., 1982; Wrigglesworth, 1984; Kumar et al., 1984a). Complex kinetic patterns associated with peroxide effects on the α-band have also been reported (Kumar et al., 1984a; Bickar et al., 1985).

To find an explanation for these variable effects, we noted that most of the studies cited above were performed at pH

† This investigation was supported by American Heart Association, Illinois Affiliate, Grant C-03 and by Biomedical Research Grant Program Award BRSG S07 RR07176, Division of Research Resources, National Institutes of Health.
* Address correspondence to this author.

0006-2960/91/0430-5727$02.50/0